Science Advances

AAAS

advances.sciencemag.org/cgi/content/full/3/9/e1701114/DC1

Supplementary Materials for

Rubbery electronics and sensors from intrinsically stretchable elastomeric composites of semiconductors and conductors

Hae-Jin Kim, Kyoseung Sim, Anish Thukral, Cunjiang Yu

Published 8 September 2017, *Sci. Adv.* **3**, e1701114 (2017)
DOI: 10.1126/sciadv.1701114

This PDF file includes:

Calculation of μ_{FE} and V_{th}

To calculate the field effect mobilitiy (μ_{FE}), we use the measured plot of the $I_{ds}^{1/2}$ versus V_{gs} and extract the mobility value based on the following equation

$$I_{ds} = \left(\frac{WC_i}{2L}\right)\mu_{FE}(V_{gs} - V_{th})^2 \quad \text{(S1)}$$

where L, W, and C_i are the channel length, the width, and the gate capacitance per unit area, correspondingly. The threshold voltage (V_{th}) is defined as the voltage where the linear regime of the curve extends and intercept with the V_{gs}. On the basis of the measured transfer curve, μ_{FE} and threshold voltage (V_{th}) can be obtained.

Optimized P3HT weight composition in P3HT-NF/PDMS composites

To validate why the composite with 20 wt% of P3HT weight composition is chosen, composites with higher weight compositions are also studied for the comparison purposes. We compared P3HT-NF/PDMS composites with different weight compositions for 20, 50, and 90 wt%. As shown in fig. S4, we present the optical microscope images, TFT transfer curves with and without mechanical stretching, and the μ_{FE} for each composite.

Upon stretching up to 50% mechanical strain, significant decrease in the μ_{FE} with an increase of P3HT weight composition was observed (fig. S4D). Specifically, the μ_{FE} for 90 wt% P3HT weight composition decreased from 2.7 $cm^2/V{\cdot}s$ to 0.1 $cm^2/V{\cdot}s$ (96% decrease) while TFT with 50 wt% P3HT weight composition decreased from 1.1 $cm^2/V{\cdot}s$ to 0.2 $cm^2/V{\cdot}s$ (82% decrease). This decrease in the μ_{FE} with an increase of P3HT weight composition is attributed to a significant amount of microcracks. For the 20 wt% P3HT weight composition, only 40% decrease in the μ_{FE} was obtained which is attributed to no obvious cracks (fig. S4A). To obtain semiconductor composite with the moderate μ_{FE} decrease and without microcracks while stretching, we therefore choose the one with 20 wt% of P3HT weight composition.

Calculation of temperature coefficient of resistance

The curve of relative resistance change (R/R_o) with regards to the temperature (T (K)) was fitted by using OriginPro® software. Based on the thermistor characteristics, the fitted curve uses the exponential decay function with the formula as following

$$R/R_o = \mathrm{A} + Be^{-CT} \quad \text{(S2)}$$

Based on Fig. 3h, the obtained fitting parameters A, B and C in the fitted curve (black line) are shown in the following table.

	Value	Standard Error
A	0.44	0.0092
B	3.92×10^5	1.25×10^5
C	0.044	0.001

Due to nonlinear characteristics of the relative resistance decrease with an increase of the temperature, the temperature coefficients of resistance (TCR) at 303 K (30 °C), 313 K (40°C) and 323 K (50°C), were calculated by using the differentiated function of the fitted curve as follows

$$\frac{\mathrm{d}(\mathrm{R}/R_o)}{\mathrm{dT}} = \frac{1}{R_o} \cdot \frac{\mathrm{dR}}{\mathrm{dT}} = -17400e^{-0.044T}$$

$$\mathrm{TCR} = \frac{1}{R} \cdot \frac{dR}{dT} = \frac{R_o}{R} \cdot \left(\frac{1}{R_o} \cdot \frac{dR}{dT}\right) \quad \text{(S3)}$$

The obtained TCR values at 303 K (30°C), 313 K (40°C) and 323 K (50°C) are –0.028/K, –0.023/K and –0.016/K, respectively.

Calculation of Hertzian contact pressure

The applied pressure to the sensor was calculated based on Hertzian contact model. When a sphere with radius R is indented into an elastic flat rubber to depth d, the radius of the contact area can be defined as $a = \sqrt{Rd}$. The applied force F as a function of d can be expressed as the following (*47*)

$$\mathrm{F} = \frac{4}{3}E^* R^{1/2} d^{3/2} \quad \text{(S4)}$$

where $\frac{1}{E^*} = \frac{1-\nu_1^2}{E_1} + \frac{1-\nu_2^2}{E_2}$, and the E_1, E_2, ν_1, ν_2 are the elastic moduli and poisson's ratios of the sphere (that is, glass) and the rubber (that is, PDMS). The modulus E_1 and possion's ratio ν_1 of the PDMS are 1 MPa and 0.5 (*32*). The modulus E_2 and possion's ratio ν_2 of the glass are 70 GPa and

0.25 (*46*). The normal pressure distribution along the contact area of radius r can be expressed as (*47*)

$$\mathrm{p(r)} = p_o \left(1 - \frac{r^2}{a^2}\right)^{1/2} \quad \text{(S5)}$$

Therefore, the maximum contact pressure can be given by

$$p_o = \frac{3F}{2\pi a^2} \quad \text{(S6)}$$

Sign language translation program

The actual translation from the electrical resistance change to the sign language letters is demonstrated based on a custom-built software using Matlab® (details in fig. S12). The logic of the software is displayed in the flowchart (fig. S12A). First, electrical resistance at each bending angle is averaged. Second, the averaged values (m) are classified into 4 different color groups, that is, blue (m < 0.9 GΩ), green (0.9 GΩ ≤ m ≤ 1.1 GΩ), pink (1.2 GΩ ≤ m ≤ 1.4 GΩ) and red (1.4 GΩ < m). Third, the set of averaged values is compared with the predetermined values of the sign language letters. Finally, all the results are displayed in graphic user interface (GUI) program to effectively understand the translation process. GUI program is comprised of a) data selection from the input, b) signal interpretation, c) color mapping and d) translated letter display window as shown in fig. S12B. The representative images in fig. S12C are the screenshots of the executed program after translating the electrical resistance response to sign language letters “YULAB”. Simultaneously, our program also contains a script to automatically display all the translated letters (fig. S12D).

Supplementary Figures

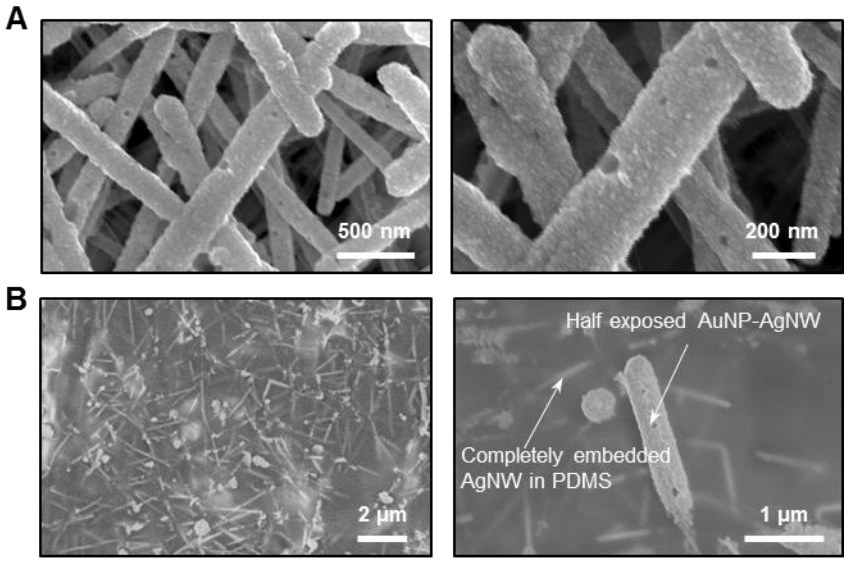

fig. S1. Fabrication of AuNP-AGNW by using a galvanic replacement process. SEM images with different magnification of AuNP-AgNWs (**A**) on a Si substrate and (**B**) embedded in PDMS.

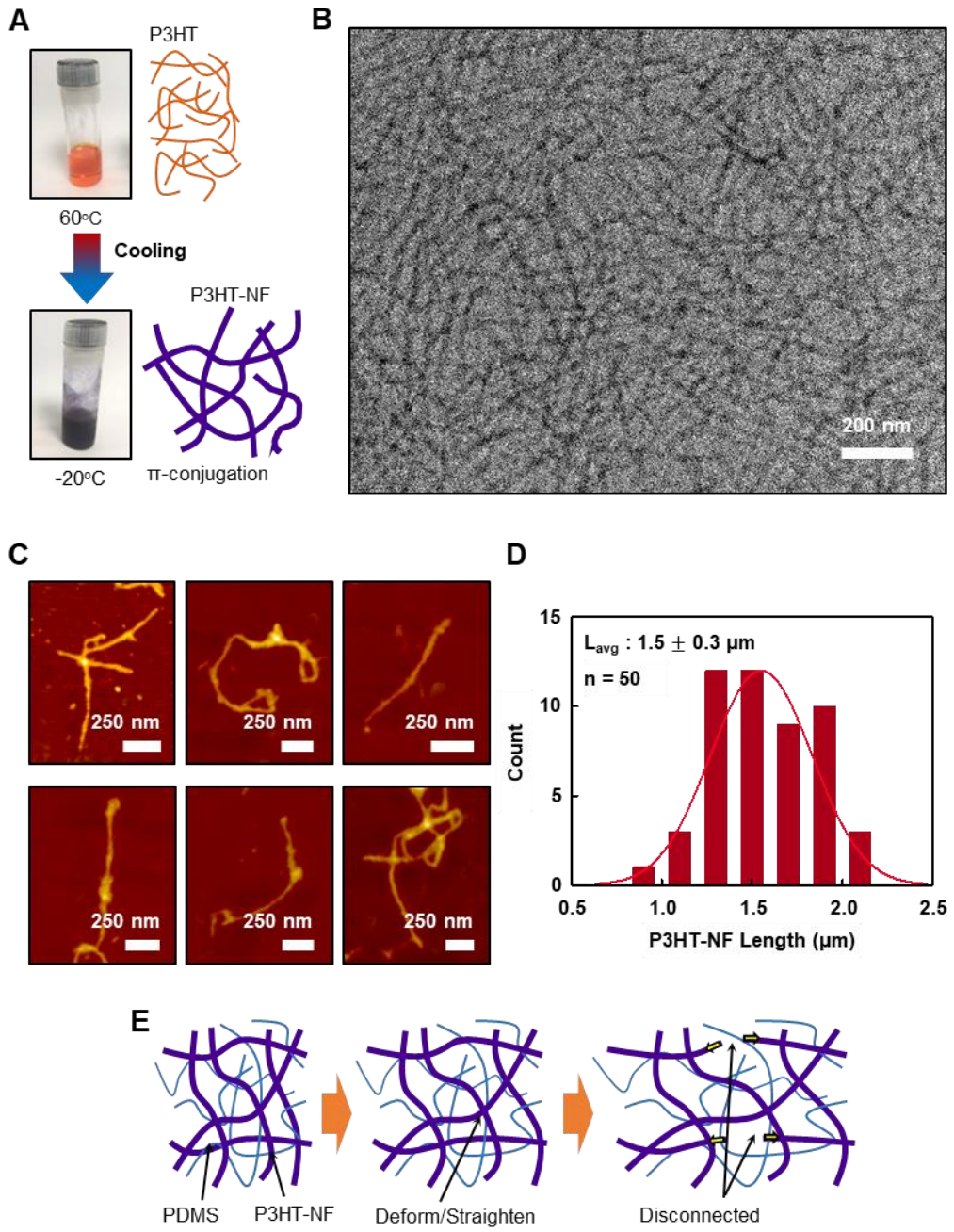

fig. S2. Fabrication and deformed states of the elastomeric composite semiconductor. (**A**) Schematic illustration of the P3HT-NF growth by using the cooling process. (**B**) TEM image of P3HT-NF. (**C**) AFM images of P3HT-NF and (**D**) Corresponding length distributions of P3HT-NF. (**E**) Schematic illustration of how the P3HT-NFs behave in the composite upon stretching.

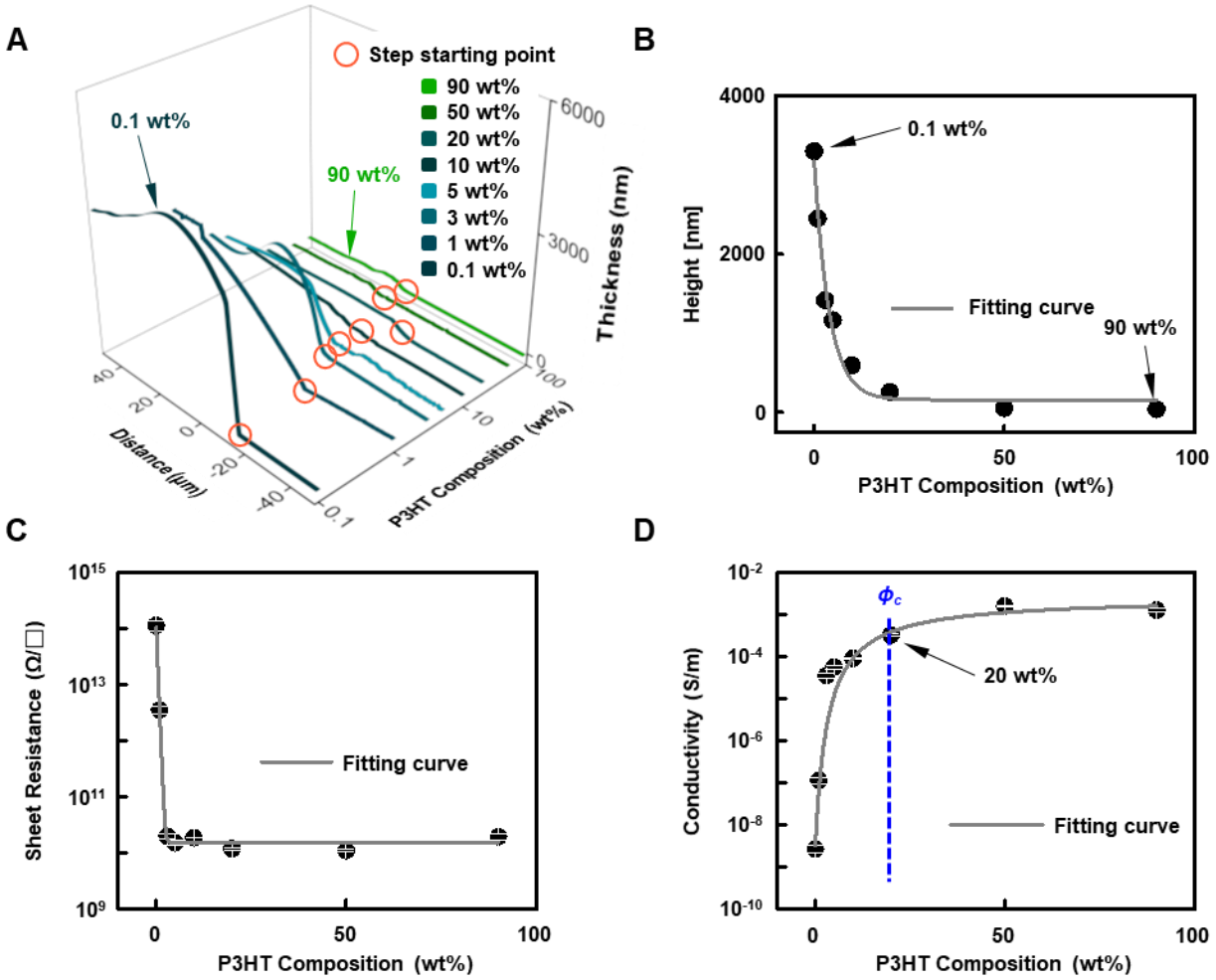

fig. S3. Percolation behavior of the P3HT-NF/PDMS composite semiconductor. (**A**) AFM scanning thickness profiles and (**B**) thickness plot of P3HT-NF/PDMS composites with different P3HT weight compositions. (**C**) Sheet resistance (Ω/□) and (**D**) conductivity (S/m) of P3HT-NF/PDMS with different P3HT weight compositions. ϕ_c indicates the percolation threshold.

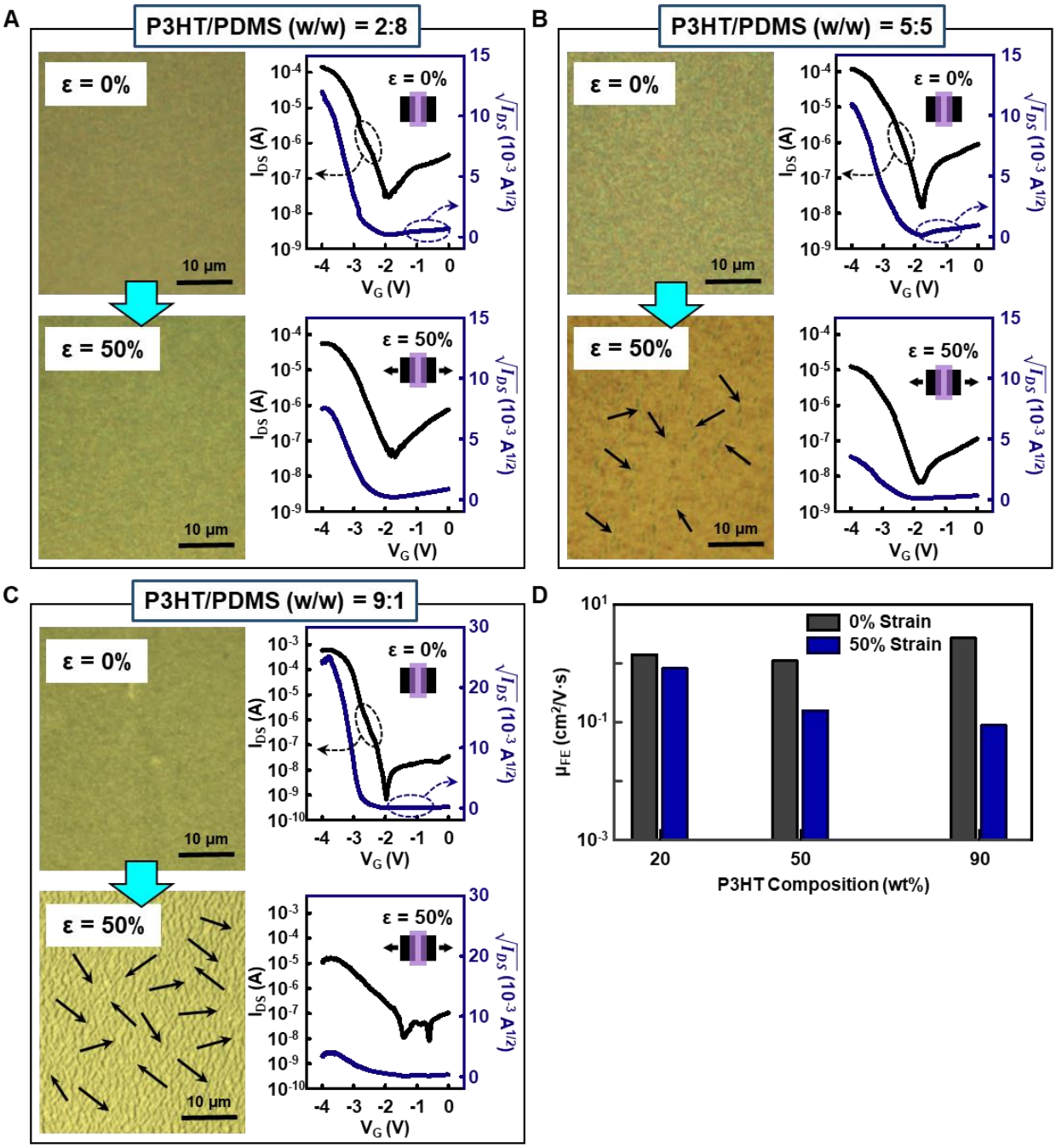

fig. S4. The composites with different weight compositions of P3HT and PDMS. Optical microscope images (left) and TFT transfer curves (right) of P3HT-NF/PDMS composites on a PDMS substrate before (upper) and after (lower) stretching to 50% with different weight composition ratio (**A**) 2:8, (**B**) 5:5 and (**C**) 9:1. The arrows in the optical microscope images indicate microcracks upon stretching. (**D**) Field-effect mobility, μ_{FE}, of the TFTs with different P3HT weight compositions under 0% and 50% of mechanical strain along the channel length direction.

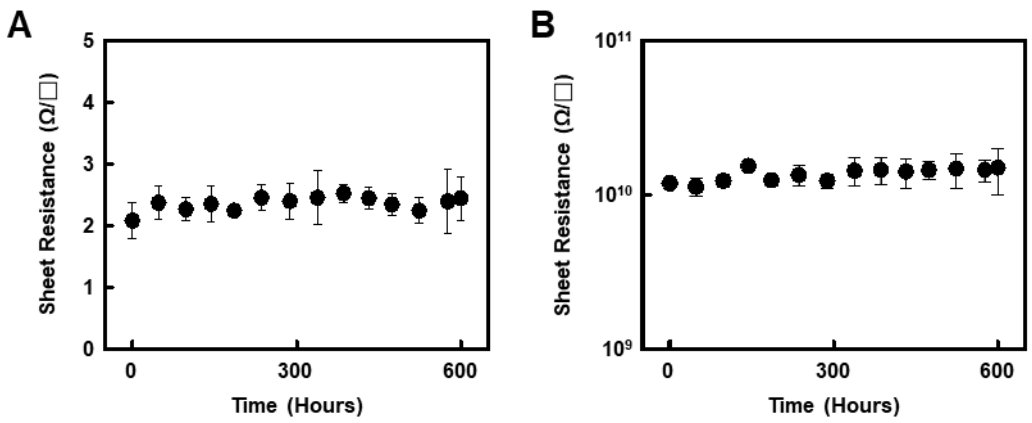

fig. S5. Lifetime of the elastomeric composite conductor and semiconductor. Sheet resistance (Ω/□) of the (**A**) AuNP-AgNW/PDMS conductor and (**B**) P3HT-NF/PDMS semiconductor stored in ambient conditions (27ºC, 50 RH%) with respect to time.

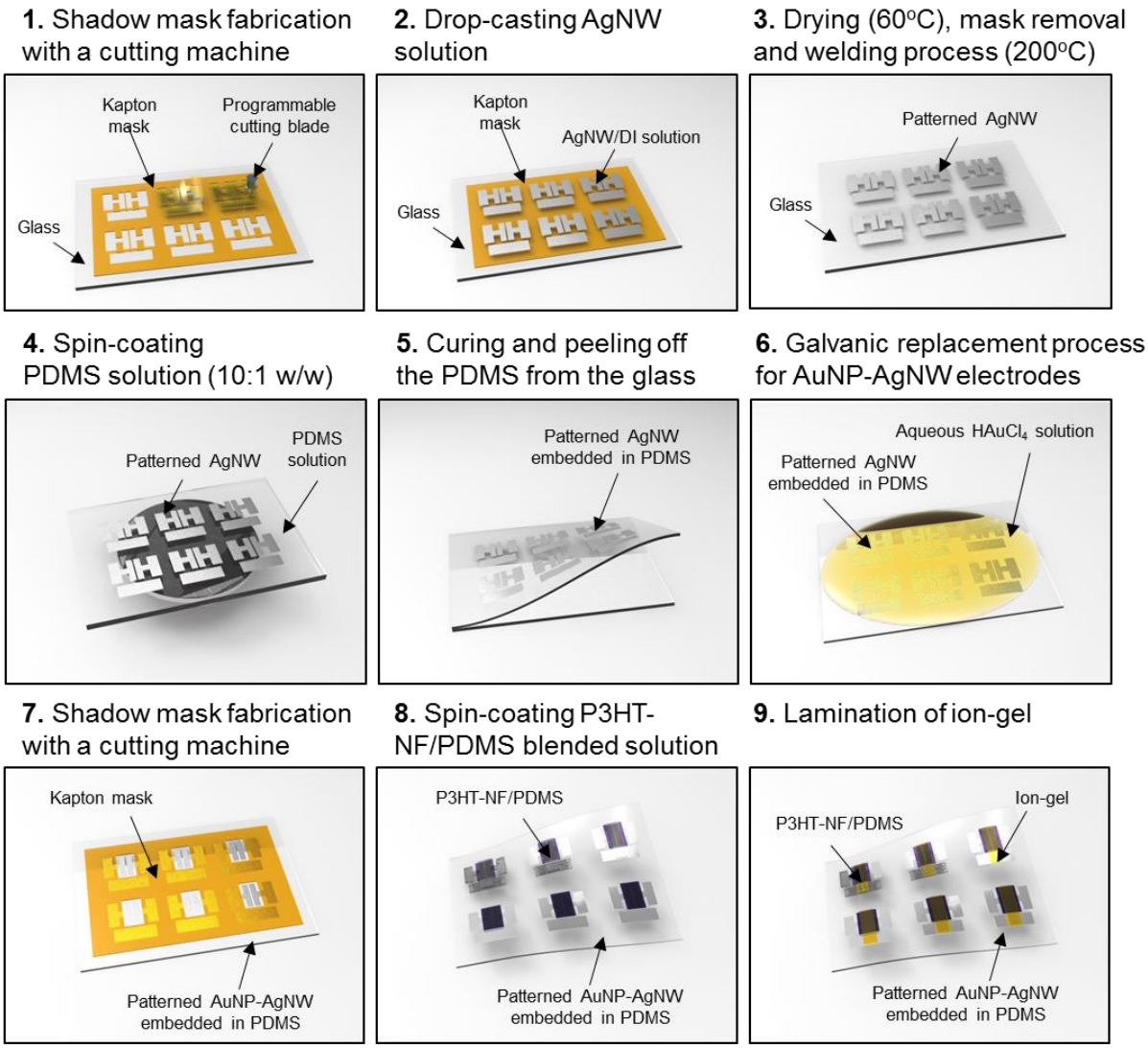

fig. S6. Fabrication steps of the intrinsically stretchable TFTs and sensors.

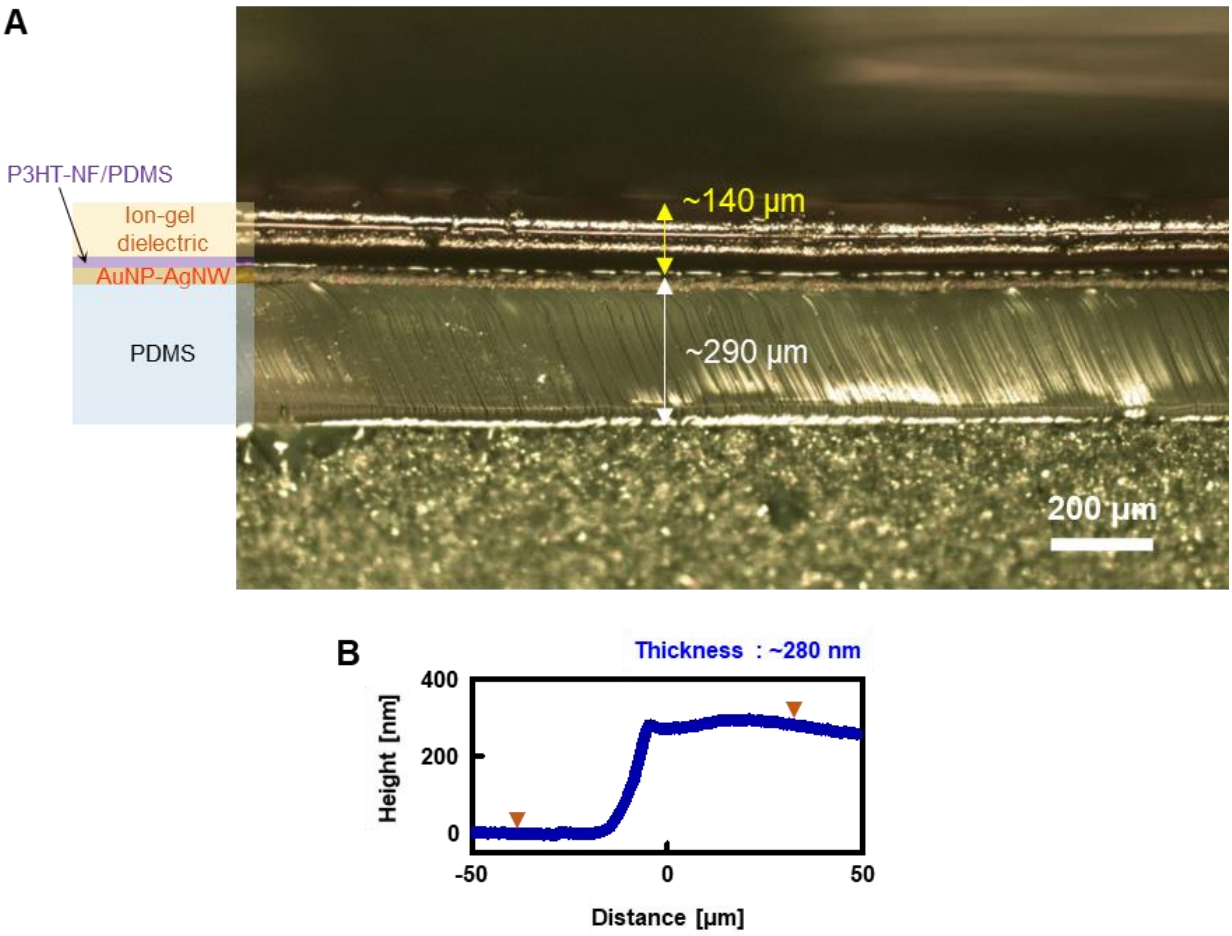

fig. S7. Thickness of the rubbery TFT and P3HT-NF/PDMS semiconductor composite. (**A**) Optical microscope image of the cross section of the rubbery TFT. (**B**) AFM scanning thickness profiles of the P3HT-NF/PDMS (2:8) composite.

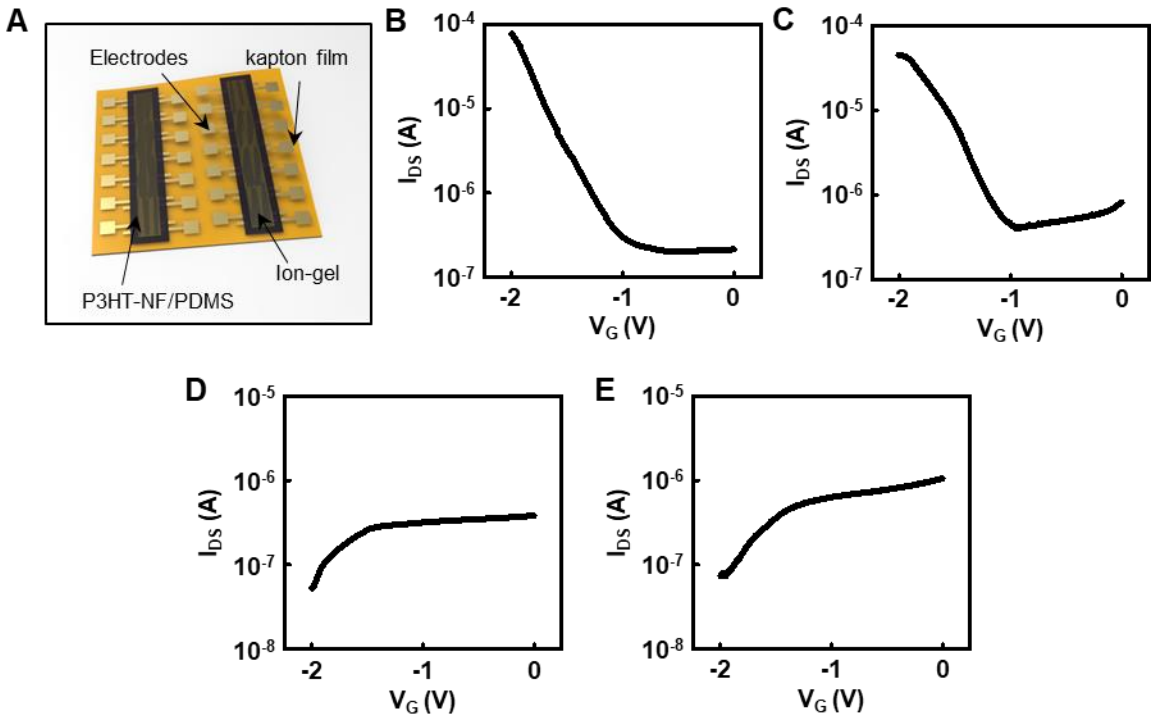

fig. S8. P3HT-NF/PDMS composite–based TFTs with different electrodes. (**A**) Schematic illustration of TFTs. (**B** and **C**) Transfer curves of TFTs with (**B**) Au and (**C**) AuNP-AgNW electrodes. (**D** and **E**) Transfer curves of TFTs with (**D**) Ag and (**E**) AgNW/PDMS electrodes.

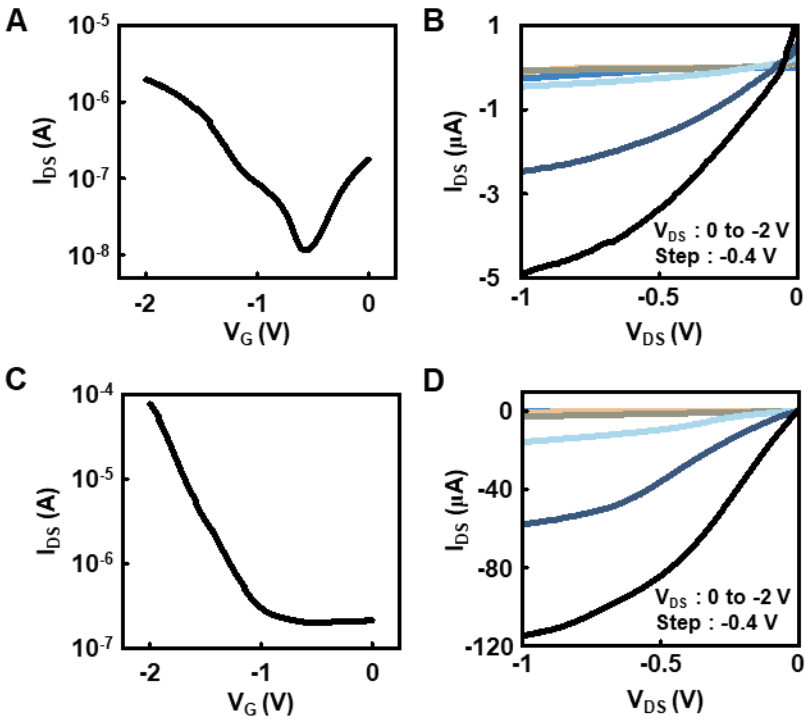

fig. S9. Performances of TFTs based on p-P3HT/PDMS and P3HT-NF/PDMS as semiconducting channels. (**A**) Transfer and (**B**) output curves of the TFT based on p-P3HT/PDMS. (**C**) Transfer and (**D**) output curves of TFT based on P3HT-NF/PDMS.

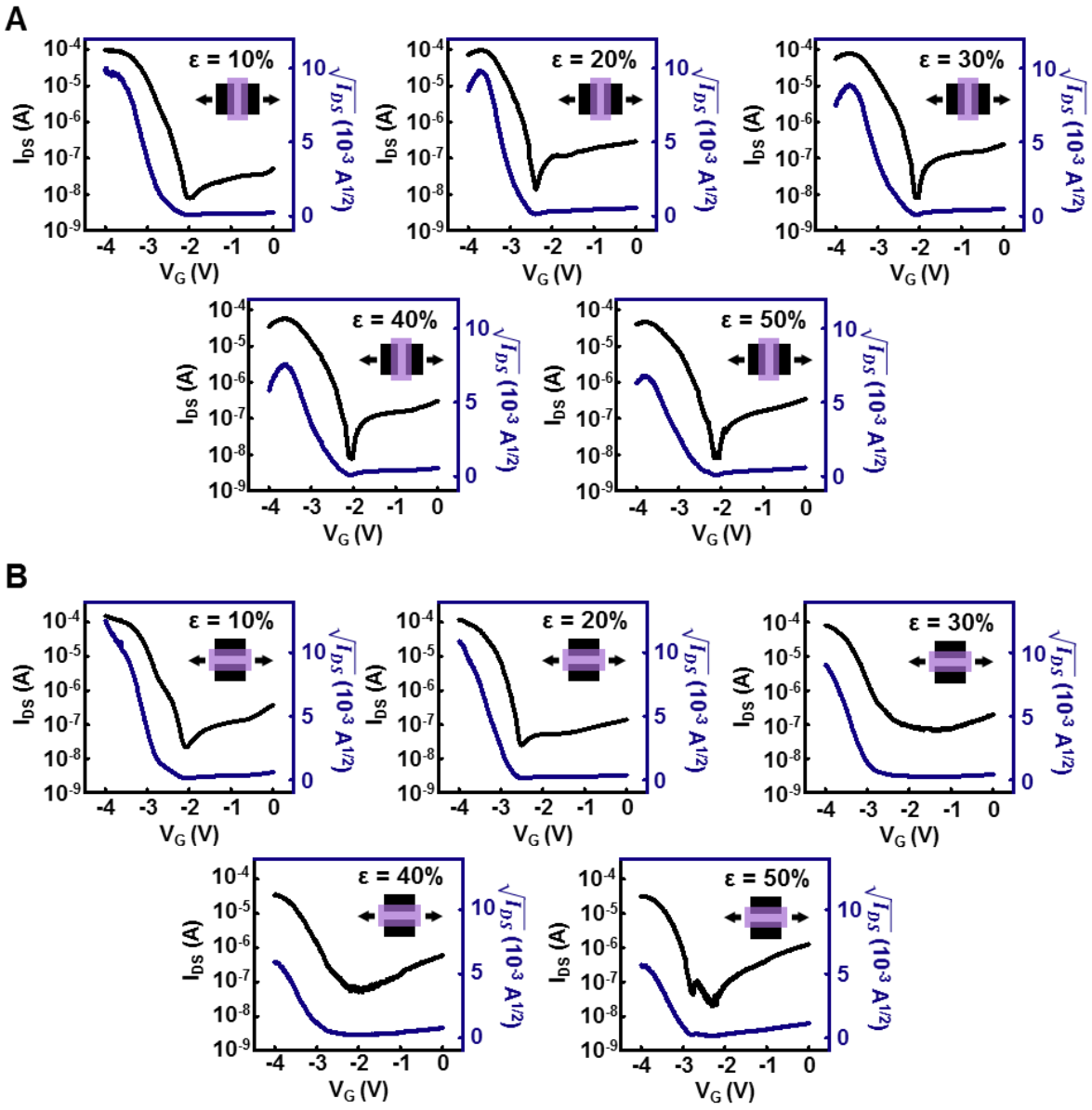

fig. S10. TFT performances with respect to mechanical strain. Transfer curves of the intrinsically stretchable rubbery TFTs under different levels of mechanical strain (**A**) along and (**B**) perpendicular to the channel length directions.

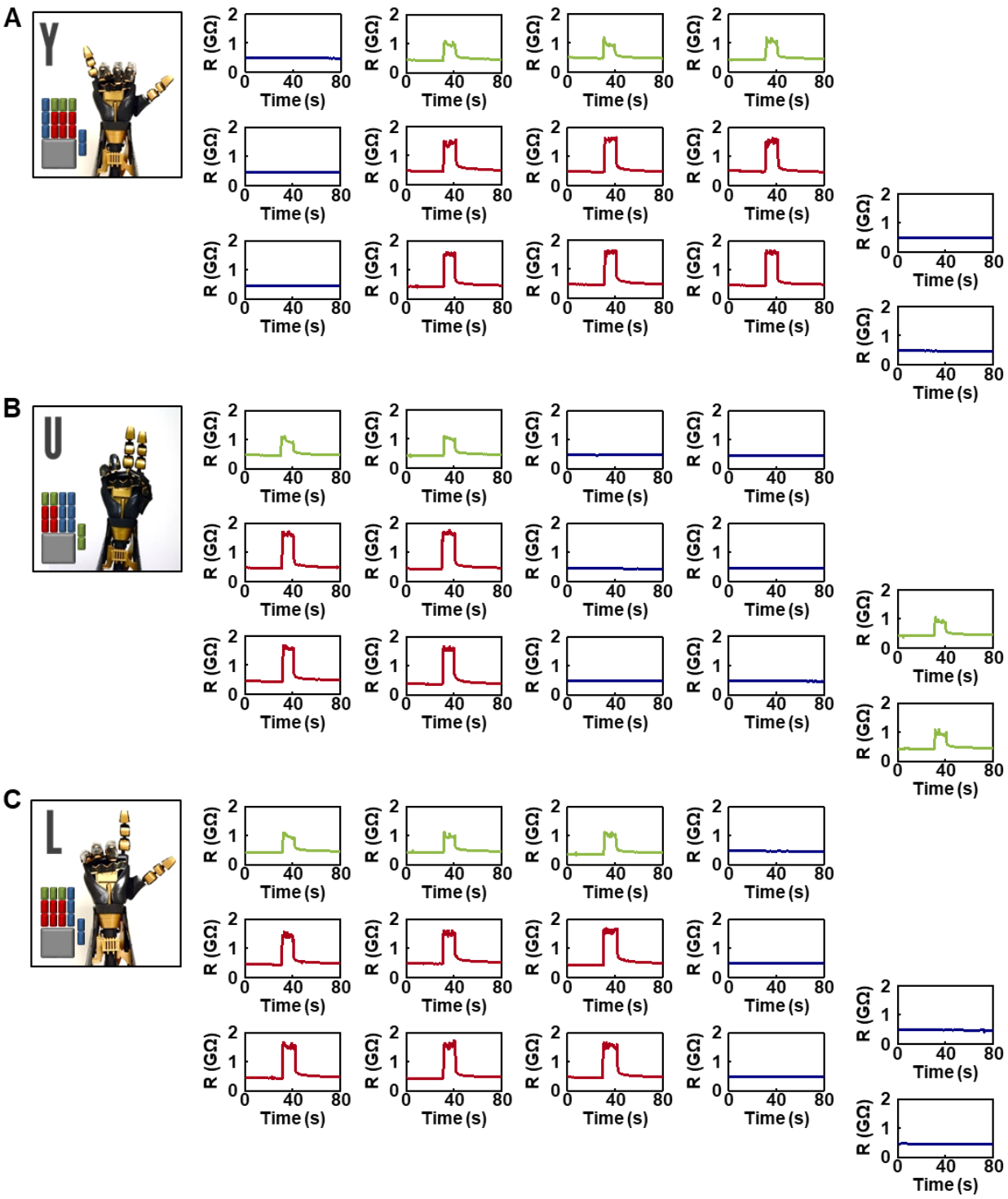

fig. S11. (Continued)

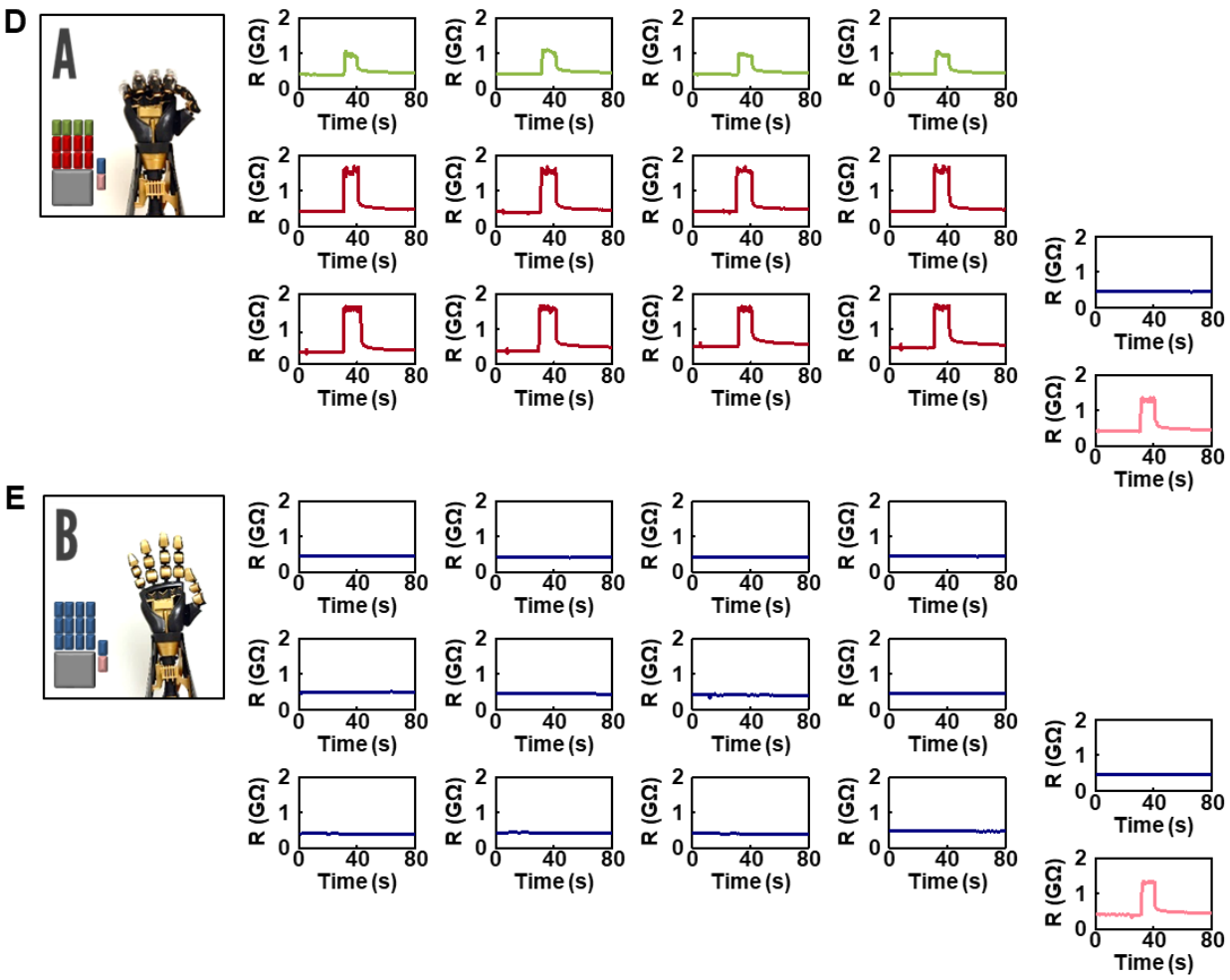

fig. S11. Electrical resistance response of the strain sensor under a given hand gesture. (**A** to **E**) Electrical resistance response of the strain sensors under a given hand gesture for the expression of the sign language letter of (**A**) Y, (**B**) U, (**C**) L, (**D**) A, and (**E**) B.

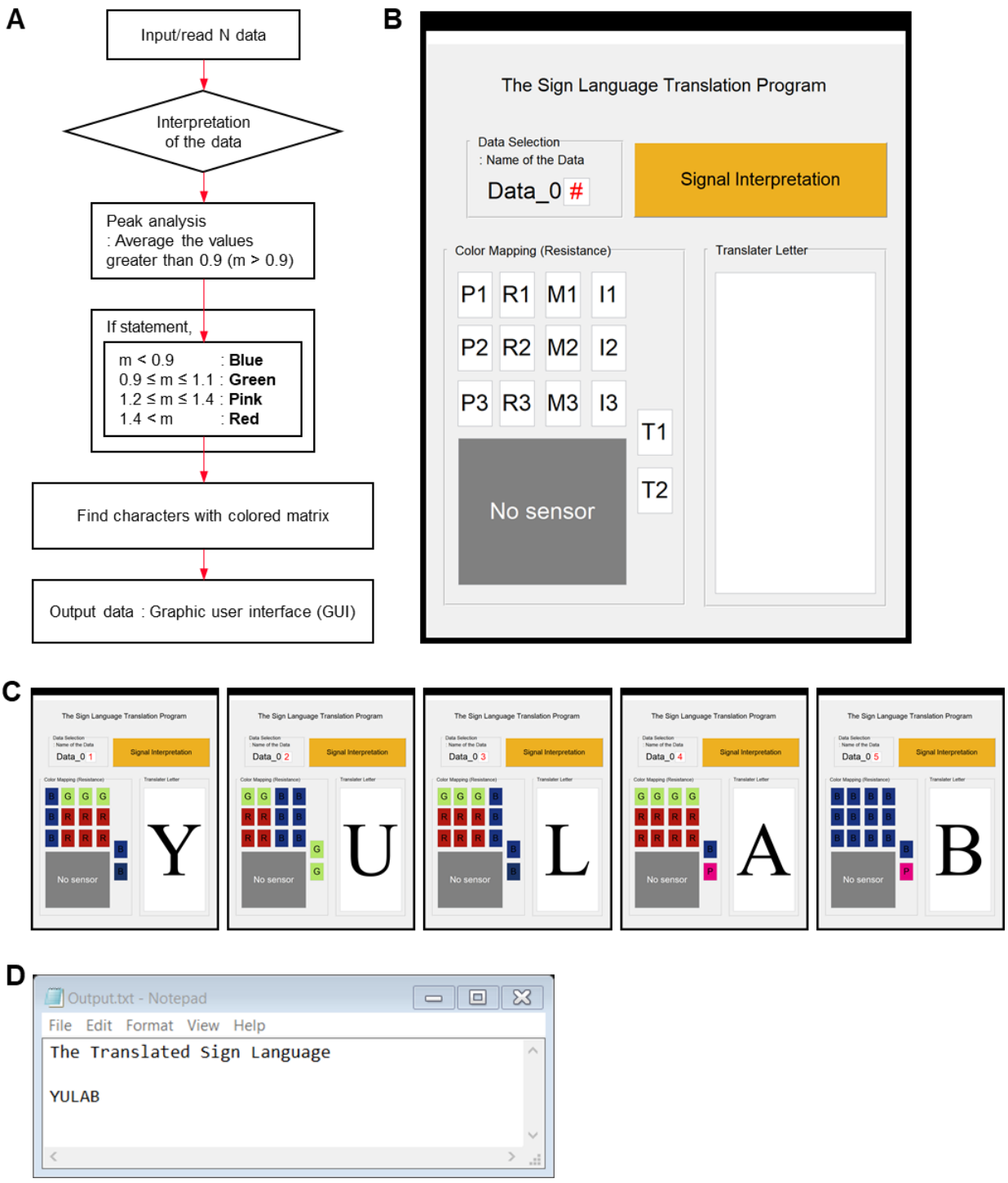

fig. S12. The sign language translation program. (**A**) Flowchart and (**B**) corresponding graphic user interface (GUI) program (.exe) for translating the electrical resistance response to sign language letters developed by using Matlab®. (**C**) Captured images of executed program after translating the electrical resistance response to the sign language letters 'YULAB' (from left to right). (**D**) Automatically generated output file (.txt).